Applied Surface Science 518 (2020) 146184

Contents lists available at ScienceDirect

Applied Surface Science

journal homepage: www.elsevier.com/locate/apsusc

Full Length Article

Hydrothermal crystallization of bismuth oxybromide (BiOBr) in the presence of different shape controlling agents

Enikő Bárdos[a,b,1], Viktória Márta[a], Lucian Baia[c,d,e], Milica Todea[d,f], Gábor Kovács[b,d], Kornélia Baán[a], Seema Garg[g], Zsolt Pap[b,d,e,*], Klara Hernadi[a,*]

[a] Department of Applied and Environmental Chemistry, University of Szeged, Rerrich Béla tér 1, HU-6720 Szeged, Hungary
[b] Institute of Environmental Science and Technology, University of Szeged, Tisza Lajos krt. 103, HU-6720 Szeged, Hungary
[c] Faculty of Physics, Babeș–Bolyai University, M. Kogălniceanu 1, RO–400084 Cluj–Napoca, Romania
[d] Nanostructured Materials and Bio-Nano-Interfaces Center, Institute for Interdisciplinary Research on Bio-Nano-Sciences Babeș-Bolyai University, Treboniu Laurian 42, RO–400271 Cluj-Napoca, Romania
[e] Institute of Research-Development-Innovation in Applied Natural Sciences, "Babeș-Bolyai" University, Fântânele 30, RO-400294 Cluj-Napoca, Romania
[f] Department of Molecular Sciences, Faculty of Medicine, Iuliu Haţieganu University of Medicine and Pharmacy, Victor Babeș 8, RO–400012 Cluj-Napoca, Romania
[g] Department of Chemistry, Amity Institute of Applied Sciences, Amity University, Sector-125, Noida 201313, Uttar Pradesh, India

ARTICLE INFO

Keywords:
Bismuth oxybromide
Photocatalytic activity
Surfactants
Rhodamine B
Surface tension

ABSTRACT

Bismuth oxybromide samples were synthesized using solvothermal crystallization and different additives (CTAB-cetyltrimethylammonium bromide, PVP–polyvinylpyrrolidone, SDS–sodium dodecyl sulfate, U–urea and TU–thiourea). The effect of the mentioned compounds was investigated through structural (crystallite size, crystal phase composition, etc.), morphological (crystal shape), optical (band gap energy) parameters, surface properties (surface oxidation states), and the resulting photocatalytic activity. It was found that the ratio of the (1 0 2)/(1 1 0) crystallographic planes, the presence of oxidized Bi^{4+} and Bi^{5+} species were responsible for the obtained photocatalytic activity. Moreover, a strong dependency was revealed between the surface tension of the shape tailoring agents and the overall morpho-structural parameters, pointing out the fact that the properties of the semiconductor can be more easily tuned using the surface tension modification as a tool.

1. Introduction

Bismuth based photocatalysts are a new generation of semiconductor materials, which can have promising photocatalytic applicability. The most important ones are bismuth oxide [1] bismuth tungstate (Bi_2WO_6) [2], bismuth vanadate ($BiVO_4$) [3], bismuth molybdate (Bi_2MoO_6) [4] and bismuth oxyhalides (BiOX, where X = Cl, Br, I) [5,6]. Recently, bismuth oxyhalides have been intensively examined, due to their unique layered structure and narrow band gap, they can have increased photocatalytic efficiency [7]. Their structure is composed of $[Bi_2O_2]^{2+}$ sheets and enclosed double-layered halogen anions can be found bonded through van der Waals interactions. When irradiated with UV or visible light, this structure forms an induced dipole, which can separate the photogenerated electron-hole pairs efficiently [8]. Among the BiOX materials, BiOBr has advantageous properties, like narrow bad gap, chemically stable or the aforementioned unique crystal structure, which makes BiOBr a suitable photocatalyst [9].

The crystallographic planes (0 0 1),(1 0 2) and (1 1 0) of BiOBr were those which were investigated in detail recently and it was found, that (1 0 2) showed lower conduction band minimum and higher valence band maximum and compared with (0 0 1). Therefore, it has electron transmission with increased efficiency, with a higher redox potential of the photoinduced hole a smaller band gap as well (1.44 eV) [10]. The (0 0 1) facet dependent photoactivity of BiOBr single crystals has also been studied in comparison with (1 1 0) and it was found that it can possess a stronger internal electric field, which could increase the recombination time of the photoinduced electron-hole pairs [11].

Several methods are available to synthesize BiOBr, such as microwave-assisted crystallization [12], hydrolysis [13] or hydrothermal synthesis [14]. Using additives during the hydrothermal synthesis, it can change the morphology [15], the mean primary crystallite size, the hierarchical particle size and shape [16], the band gap energy values [17] or the specific surface area [18], thus increase the efficiency of the photocatalytic degradation of organic pollutants. Polyvinylpyrrolidone

* Corresponding authors at: Institute of Environmental Science and Technology, University of Szeged, Tisza Lajos krt. 103, HU-6720 Szeged, Hungary (Z. Pap). Department of Applied and Environmental Chemistry, University of Szeged, Rerrich Béla tér 1, HU-6720 Szeged, Hungary (K. Hernádi).
E-mail addresses: pzsolt@chem.u-szeged.hu, pap.zsolt@phys.ubbcluj.ro (Z. Pap), hernadi@chem.u-szeged.hu (K. Hernadi).
[1] 1st author.

https://doi.org/10.1016/j.apsusc.2020.146184
Received 22 January 2020; Received in revised form 18 March 2020; Accepted 21 March 2020
Available online 24 March 2020

(PVP) [19], sodium dodecyl sulfate (SDS) [16] or cetyl trimethylammonium bromide (CTAB) [20] are among those additives, which were already used as shape-tailoring agents.

SDS, CTAB and PVP molecules have a hydrophilic (SDS – sulfate group; CTAB – ammonium group, PVP – pyrrolidone group) and a hydrophobic group (SDS and CTAB – hydrocarbon group, PVP – hydrocarbon backbone). The hydrophilic groups of these molecules could attach selectively on the surface of the crystallographic planes of the BiOBr and control the epitaxial growth of the crystal facets, thus controlling the morphology and the crystal size finally. On the other hand, the presence of a hydrophobic functional group can regulate the distance among the adsorbed hydrophilic functional groups and control the thickness of the nanosheets [21].

According to the scientific literature, using PVP as an additive could result in a growth favouring the (1 1 0) crystallographic plane, instead of (1 0 2) or (1 0 1) [22]. Moreover, it was already proved, that using PVP during the hydrothermal crystallization of BiOBr could change the morphology, increase the specific surface area and decrease the band gap energy, because it could reduce the surface tension, stabilize the metal nanoparticles, resulting in higher efficiency of photodegradation toward the selected organic contaminant (methyl orange) [21]. Interestingly, using SDS as the additive could induce the appearance of oxygen vacancies in the crystal structure of BiOBr [23] and it could change the morphology of BiOBr as well from microflowers to hollow structured microspheres [24]. CTAB was used in the synthesis of BiOBr both as Br source and shape tailoring agent in aqueous solution [25] and in the presence of urea [26].

A similar effect on the morphology was noticed using urea as the additive, like in the presence of PVP or SDS, while the appearance of oxygen vacancies was observed as well [27]. Urea and thiourea were already used as doping agents during the hydrothermal synthesis of BiOBr in 3-methoxyethanol and solution and the as-obtained semiconductor successfully enhanced the photocatalytic decomposition of Rhodamine B [28]. On the other hand, to the best knowledge of the authors, it is not discussed in detail, whether thiourea or urea used as surfactants has influence on the properties of BiOBr, but it seems from the few available papers that it is indeed important, as it was shown systematically for other bismuth-based material, namely the bismuth tungstate (Bi_2WO_6) [29].

Therefore, considering the aspects mentioned above, the solvothermal crystallization method was used to obtain BiOBr in the presence of different additives, namely CTAB, SDS, PVP urea and thiourea, respectively and this study CTAB was used as a shape controlling agent. Hence, our main aim was to compare the effect of the different additives on the crystal structure, morphology, band gap energy, surface tension of the synthesis mixture and to investigate the photocatalytic activity of the as-obtained semiconductors towards Rhodamine B.

2. Materials and methods

2.1. Synthesis

Bismuth oxobromide (BiOBr) materials were prepared by the solvothermal crystallization method. For the synthesis 2.36 g Bi$(NO_3)_3{\cdot}5H_2O$ (VWR, 98.0%) was dissolved in of 50 mL ethylene glycol (VWR Chemicals, 99.5%), and 0.2 g of shape-tailoring agent such as polyvinylpyrrolidone (PVP K30 abbreviated as PVP) (Molar Chemicals 99%), sodium dodecyl sulfate (SDS) (Biolab 98%), cetyl trimethylammonium bromide (CTAB) (Sigma Aldrich, 98%), urea (U) (Molar Chemicals 99%) or thiourea (TU) (Sigma Aldrich, 99%) was added to the solution (to manipulate the surface tension, Table 1). Afterwards, 0.58 g (Bi:X = 1:1) of KBr (VWR 99.0%) was also added. The solution was kept at 50 °C for 15 min and then transferred to a Teflon® lined autoclave which was placed in an oven (Binder BD 115) at 120 °C for 3 h. After the synthesis finished, the autoclave was cooled down to room temperature. The precipitate was washed with 0.5 L of distilled water and 0.5 L ethanol (VWR, 96%) using a vacuum filter. The as-prepared samples were dried at 40 °C for 12 h. The nomenclature of the materials was derived as follows: *BiOBr _ applied additive*.

Table 1
The surface tension of the additives in ethylene glycol.

Additives	Surface tension ($N{\cdot}m^{-1}$)
Ethylene glycol (EG)	0.05378
EG + CTAB	0.05086
EG + SDS	0.06483
EG + PVP	0.06111
EG + U	0.05865
EG + TU	0.05405

2.2. Characterization methods

To measure the optical properties of the samples, diffuse reflectance spectroscopy was applied. The (DRS) spectra of the samples were recorded using a JASCO-V650 spectrophotometer with an integration sphere (ILV-724, λ = 250–800 nm). The band gap energy values were evaluated by the Kubelka-Munk approach and the Tauc plot [30].

Hitachi S-4700 Type II FE-SEM scanning electron microscope (SEM) was used to record the micrographs. The microscope was equipped with a cold field emission source operating in the range of 5–15 kV. The samples were mounted on a conductive carbon tape, which was attached to an aluminum holder.

FEI Technai G2 X-TWIN TEM (200 kV) transmission electron microscope was used to record micrographs about the morphology of the particles. The samples were prepared as follows: a small amount of the examined materials was carried out in 1.25 cm^3 of ethanol. A few drops from this suspension were deposited and dried onto the surface of the grid (CF 200 Cu TEM grid).

Powder X-ray diffractometry (XRD) was carried out on a Rigaku Miniflex II diffractometer 2θ° = 20–60°, λ (CuK_α) = 0.15418 nm) using 2° min^{-1} scanning speed. The primary crystallite mean size values were calculated using the Scherrer equation [31].

The specific surface areas of the catalysts were determined by N_2 adsorption at 77 K, using a BELCAT-A device. The specific surface area was calculated by applying the BET method.

XPS measurements were performed on a Specs Phoibos 150 MCD system employing a monochromatic Al-Kα source (1486.6 eV) at 14 kV and 20 mA and the X-ray source with a power of 200 W, while the pressure in the analyzer chamber was lower than 10^{-12} bar. Samples were mounted on double-sided carbon tape. The high-resolution O1s and Bi4f spectra were obtained using analyzer pass energy of 20 eV in steps of 0.05 eV for analyzed samples.

The surface tension of the synthesis solution was determined by using a 3.5 mL stalagmometer and Milli-Q water as the reference. The density of the solutions was determined by using a pycnometer (10 mL) coupled on a thermometer. The following Eq. (1) was applied during the calculations:

$$\gamma = \frac{\gamma_w \cdot \rho \cdot n_w}{\rho_w \cdot n} \quad (1)$$

where γ, γ_w - the surface tension values (Pa·s)
n, n_w - the number of counted liquid drops
ρ, ρ_w – density of the liquid ($g{\cdot}cm^{-3}$)
w - short for water.

2.3. Evaluation of photocatalytic efficiency

The photocatalytic decomposition of Rhodamine B was carried out in a double-walled Pyrex® glass reactor surrounded by a thermostatic

jacket (T = 25 °C) under UV (λ_{max} ≈ 365 nm) and visible irradiation (λ > 400 nm). The reactor was surrounded by 6 × 6 W black light lamps (Fig. S1 show the spectrum of the black light lamp) (9.53 W/m^2 energy flux on the reactor position) or 4 × 24 conventional compact fluorescent lamps (Düwi 25920/R7S-24 W; 81.37 W/m^2 energy flux on the reactor position). During visible light experiments, the spectrum of the lamps was slightly modified by circulating 1 M sodium nitrite (Molar Chemicals, min. 99.13%) aqueous solution in the thermostatic jacket. The $NaNO_2$ solution absorbs any UV photons below 400 nm, providing only visible light irradiation (Fig. S2), while during the UV tests, water was the thermostatic agent. The reactor ($C_{0,RhB}$ = 0.25 mM; $C_{suspension}$ = 1.0 g·L^{-1}; total volume of the suspension $V_{suspension}$ = 130 mL) was continuously stirred and purged with air to keep the dissolved oxygen concentration constant during the whole experiment (degradation time = 2 h). 1.5 mL sample was taken in 0, 10, 20, 30, 40, 50, 60, 80, 100 and 120 min and placed into a sample holder, centrifuged for 3 min at 13,400 rpm and filtered with Filtratech 0.25 μm syringe filter. The concentration of Rhodamine B (RhB) was followed by using a JASCO V-650 spectrophotometer at a detection wavelength fixed at 554 nm.

3. Results and discussion

3.1. Evaluation of crystal phase composition and primary crystallite mean size

Fig. 1(A) shows the diffractograms of the samples, from which it can be concluded that the tetragonal structure of BiOBr (JCPDS card No. 78-0348) was obtained and no other relevant signals were present. It was also observed, that the XRD pattern of BiOBr_∅ showed sharp diffraction peaks of (1 1 0) and (1 0 2). When additives were used during the synthesis, the intensity ratios of the (1 1 0) and (1 0 2) crystallographic planes were changed. More precisely, the intensity of (1 0 2) signal decreased compared to (1 1 0) (Table 2). BiOBr_PVP and BiOBr_TU samples had the lowest relative amount of (1 0 2), compared to samples BiOBr_∅, BiOBr_U, BiOBr_SDS and BiOBr_CTAB which means that PVP and TU could adsorb on the surface of the forming BiOBr nuclei selectively and induced the (1 1 0) crystal facet growth. This observation is in good accordance with the scientific literature [21]. Interestingly, the ratio of (1 0 2)/(1 1 0) crystal facets was nearly unchanged if CTAB, SDS, and U were applied as additives.

The results suggested that the synthesis of BiOBr in the presence of surfactants showed increased primary crystallite size values compared to the reference sample (e.g.: BiOBr_∅ 12 nm *vs.* BiOBr_TU 25.3 nm) except for BiOBr_SDS which showed 11.5 nm-sized crystallites. It is well-known that decreased primary mean crystallite size could be advantageous for the photocatalytic activity because it is associated with the higher specific surface area [32].

When the (1 0 2)/(1 1 0) crystal facet ratios were considered (Fig. 1(B)) the mean primary crystallite size values changed along a maximum curve, but it can be observed, that BiOBr_SDS was an exception again, which may be attributed to other surface properties, such as oxygen vacancies or the presence of other surface species.

3.2. Morphological characterization

Using surfactants or polymers during the synthesis might cause morphological and structural changes. Therefore, the investigation of morphological properties and particle size distribution of the materials was necessary. Without any surfactants, the morphology of BiOBr showed microspherical particles, which were composed of fine nanoplates (Fig. 2). When CTAB or SDS were used, the morphology did not change significantly compared to sample BiOBr_Ø, but the average hierarchical crystal size decreased from 2.0 μm (BiOBr_Ø) to 1.3–1.4 μm (BiOBr_SDS, BiOBr_CTAB) and the crystal size distribution interval narrowed.

Investigating the morphology of BiOBr_PVP, it was found, that the microspheres have changed to “microflowers”, the arrangement of composing plates became less dense, the average hierarchical crystal size decreased from 2.0 μm to 1.2 μm, and the sample became more monodisperse compared to the BiOBr_Ø reference. The supposed reason is that (Fig. 3) the formed crystal nanoplates became thinner, which could cause the decreased primary crystallite particle size and the diminished intensity of the (1 0 2) crystallographic plane (Fig. 1).

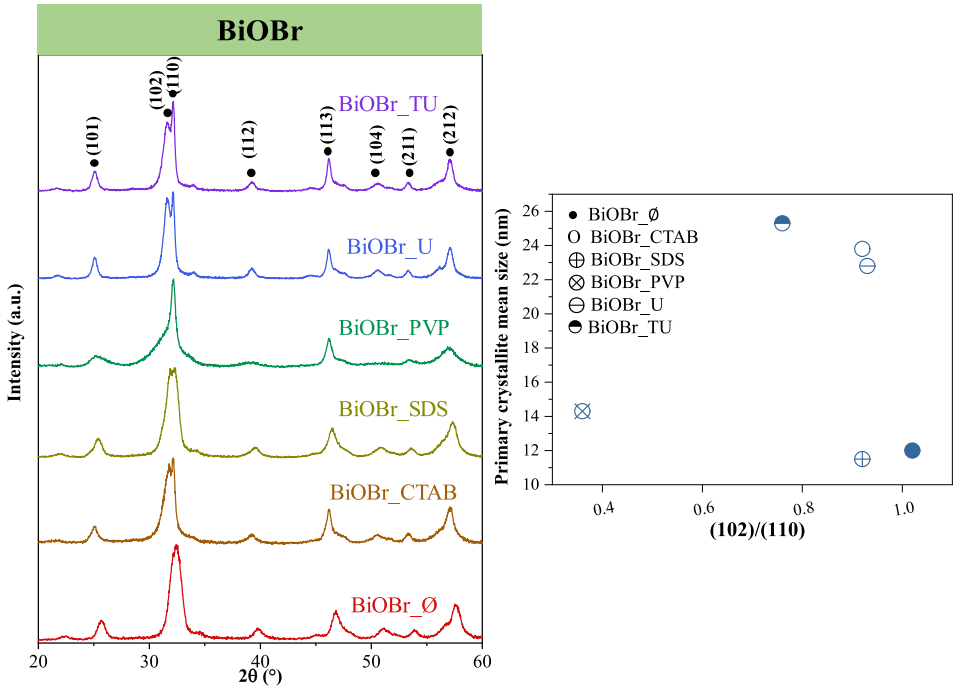

Fig. 1. X-ray diffraction patterns of BiOBr samples (A) and the correlation between the primary crystallite mean size and the (1 0 2)/(1 1 0) (B) crystallographic planes ratio.

Table 2
Morphological, structural, optical and photocatalytic properties of the BiOBr materials.

Sample name	$D_{crystallite}$ (nm) (XRD)	$D_{hierarchical}$(μm) (SEM)	Band gap (eV)	(1 0 2)/(1 1 0) ratio	S_{BET} ($m^2 \cdot g^{-1}$)	Surface tension ($N \cdot m^{-1}$)	Bi^{3+}	Bi^{4+}	Bi^{5+}	Photocatalytic conversion (%)	
							From the total amount of Bi (%)			UV	Vis
BiOBr_∅	12.0	2.0	2.85	1.00:1.00	18	0.05645	93.2	6.8	0.0	19	44
BiOBr_CTAB	23.8	1.4	2.84	0.92:1.00	14	0.05420	100.0	0.0	0.0	41	47
BiOBr_SDS	11.5	1.3	2.86	0.92:1.00	10	0.05073	100.0	0.0	0.0	33	40
BiOBr_PVP	14.3	1.2	2.96	0.36:1.00	41	0.05756	76.1	16.3	7.7	49	97
BiOBr_U	22.8	1.3	2.80	0.93:1.00	10	0.05758	89.3	8.5	2.2	14	93
BiOBr_TU	25.3	0.8	2.85	0.76:1.00	33	0.06345	91.6	5.4	3.0	41	68

It is also worth to be mentioned, that according to scientific literature using SDS or PVP during the hydrothermal treatment of BiOBr could form hollow microsphere structures [22,24], so it is required to investigate this property by TEM. When urea (sample BiOBr_U) was applied during the synthesis, the appearance of a cube-shaped hierarchical structure was noticed (Fig. 2, red frames) and the average hierarchical size decreased from 2.0 μm to 1.3 μm compared to BiOBr_Ø. When thiourea was used, the morphology changed microflower structure again, similarly when PVP was used and the average hierarchical crystal size was the smallest (0.8 μm) in the BiOBr series.

By analysing the hierarchical size distribution of the obtained BiOBr series, it was concluded, that in all cases, the size distribution became narrower compared to the BiOBr_ Ø sample (0.75–4.00 μm). The BiOBr_TU and BiOBr_PVP exhibited the smallest average diameter of the hierarchical crystal size (BiOBr_TU: 0.8 μm, BiOBr_PVP: 1.2 μm) and size distribution (BiOBr_TU: 0.5–1.5 μm, BiOBr_PVP: 0.5–2.0 μm).

Fig. 3 shows the TEM images of the obtained BiOBr semiconductor materials. As it can be seen, that BiOBr_∅, BiOBr_CTAB, BiOBr_SDS, and BiOBr_U showed solid microspherical structure and BiOBr_PVP and BiOBr_TU has similar flower-like structure, which is in good accordance with the SEM results.

From SEM and TEM investigations, it can be concluded, that using additives not only the primary crystallite mean size and crystal facet ratios can be changed, but also the morphology and the size distribution, which could affect the photocatalytic efficiency as well.

3.3. Assessment of the band gap energy values

Investigating the optical properties of the BiOBr materials, it was found that the additives did not affect the band gap significantly (Fig. 4(A)), and were similar to those published in the literature (2.7–3.0 eV) [8].

In the case of the BiOBr_U, a shoulder appeared on the light absorption edge (Fig. 4(A)), therefore the first-order derivative of the DRS spectra was evaluated. Three transition bands can be seen (Fig. 4(A) inset), two of them were responsible for the electron transitions under UV light and one for the visible light-driven electron transition. The peak 418 nm corresponded to the band gap value of the tetragonal phase of BiOBr (418 nm = 2.9 eV). The UV peak at 370 nm could be attributed as the band gap energy of $Bi_6O_6(OH)_3(NO_3)_3 \cdot 1.5\ H_2O$, while the signal at 394 nm corresponded to $Bi_2O_2(OH)(NO)_3$, both of them are considered as photocatalysts [33–35]. Thus, the presence of this material could increase the photocatalytic efficiency, as we have already proved in our previous work [36]. Supposedly, these two materials are present in sample BiOBr_U, in a small amount and for this reason, their diffraction peaks did not appear in the XRD patterns. Interestingly it was also observed, that the BiOBr_PVP sample had the highest band gap energy value (2.96 eV).

Similar to the XRD results, the connection between the ratios of crystallographic planes and the primary mean crystallite size was also investigated. The (1 0 2)/(1 1 0) crystal facet ratios were increased it caused a redshift in the band gap energy (Fig. 4(B)), which means, that the (1 0 2) crystallographic plane could lower the band gap energy, which is in good accordance with the scientific literature [10].

3.4. Photocatalytic efficiencies of BiOBr materials

After detailed characterization, the photocatalytic performance of the BiOBr materials was evaluated. Investigating the photocatalytic efficiency under UV light irradiation, it was observed that the BiOBr_PVP showed the highest photocatalytic activity which was expected based on the small hierarchical and mean primary crystallite size, the highest specific surface area (Table 1) and despite the high band gap energy. BiOBr_PVP degraded 49% of the model pollutant under UV after 120 min and 97% under visible light (Fig. 5(A) and (B)). Interestingly, higher activity was measured under visible light than under UV irradiation. However, a single exception was observed in the case of BiOBr_SDS, where despite the smallest primary crystallite mean size its activity was low both in UV and visible light. Sample BiOBr_CTAB degraded 41% of the RhB under UV and 47% under visible irradiation, respectively. BiOBr_∅, BiOBr_TU and BiOBr_U all showed lower photocatalytic efficiency under UV light (degraded only 14–41%), like under visible light irradiation (degraded 68–93%). Another interesting observation was, that the sample BiOBr_U did not show high activity under UV light (14%), but under visible light, it degraded 93% of RhB. These contradictory phenomena that most of the samples showed higher activity under visible light than UV light irradiation, might have a possible explanation: photosensitization.

The photosensitization process means that the dye adsorbs on the surface of the BiOBr and it could increase the photoabsorption and improve the efficiency of photocatalytic degradation increasing the photoexcited electrons. It was already proved, that the energy of the lowest unoccupied molecular orbital (LUMO) of RhB is 0.2 eV above of the conduction band minimum (CBM) of the BiOBr. It means that the higher LUMO energy level of the dye similar to the semiconductor's CBM and it is advantageous for electron transition (Fig. 6). The photoexcitation of RhB under visible light irradiation could result in an efficient electron transition into the conduction band of BiOBr, where it could generate radicals [10]. The photosensitization processes probably did not occur under UV irradiation, because the RhB molecules cannot be excited with the same efficiency. It was confirmed the RhB was also adsorbed on the catalysts' surface, which was also proven also by the colour change of the powder from yellowish-white to pink. Moreover, the diffuse reflectance spectra of the BiOBr samples were recorded after the degradation and a subsequent purification step and it was also confirmed that the samples were coloured (Fig. S2).

The connection between photocatalytic activity and the ratio of the crystal phases ratios were also evaluated. As can be seen in Fig. 5(C), when (1 0 2)/(1 1 0) crystal facets ratios were increased, the photocatalytic activity of BiOBr samples under UV irradiation was decreased, which means, that the (1 1 0) crystallographic plane could increase the photocatalytic activity under UV light irradiation. It was also observed that between the degradation efficiency under visible light and the (1 0 2)/(1 1 0) crystal facet ratio, no significant changes were noticed.

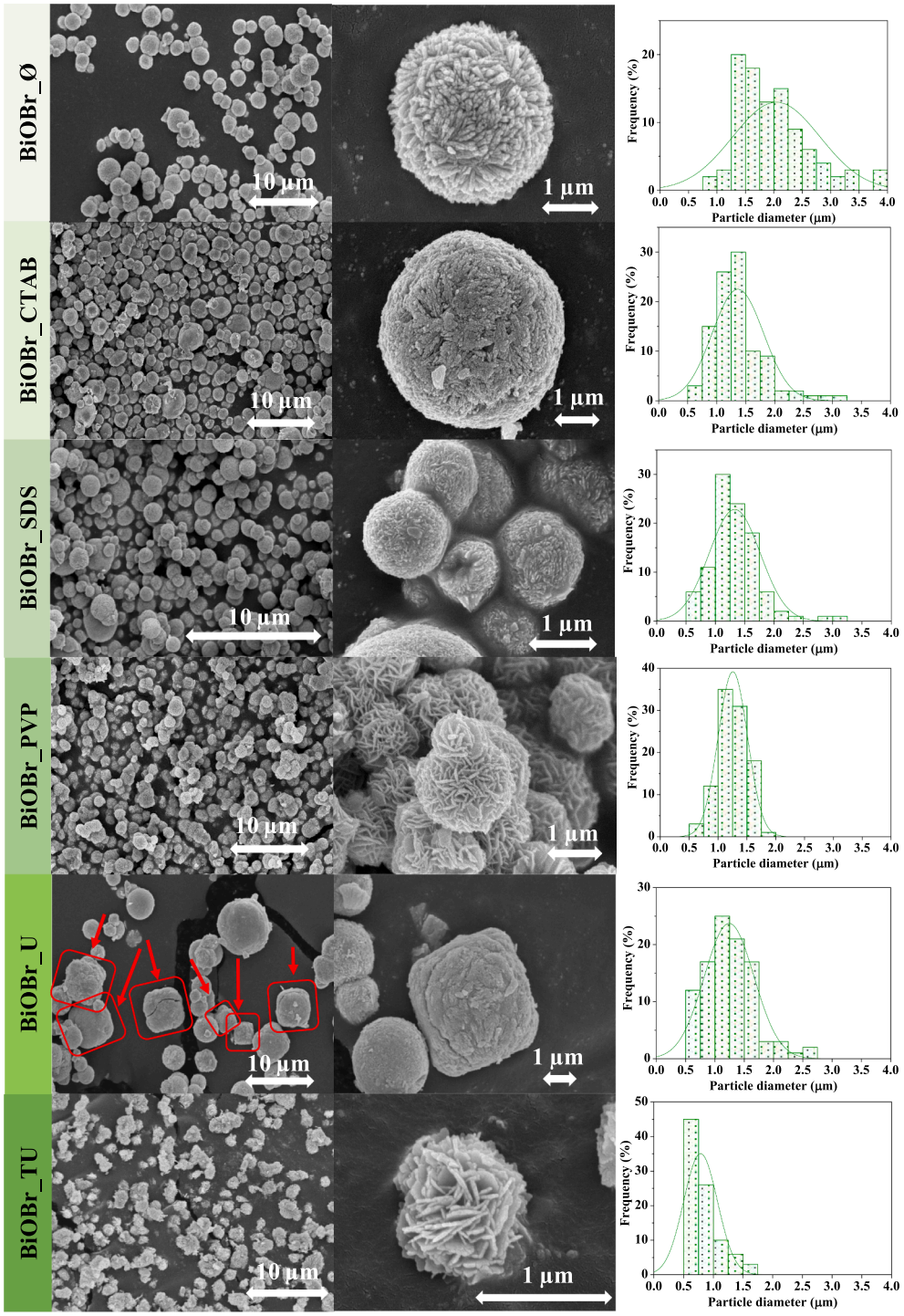

Fig. 2. The SEM micrographs and size distribution of the BiOBr semiconductor materials obtained in the presence of different shape tailoring agents.

However, a single exception was observed, the sample BiOBr_SDS, which showed lower photocatalytic efficiency.

3.5. The reason behind of the photocatalytic activity trends and the effect of the additives

The surface tension of the synthesis solution was evaluated to understand the influence of the different additives on the morphology, band gap energy, and the photocatalytic efficiency. The specific surface area of the samples increased with the surface tension but sample BiOBr_PVP was an exception, as it had the highest specific surface area and low primary crystallite size. The reason for this phenomenon was when the surface tension was higher, the formed micelles became smaller, therefore the formation of pores was facilitated. Additionally, as it can be seen that the primary crystallite mean size slightly increases when the surface tension increases confirming the correlation found with the specific surface area.

Investigating the (1 0 2)/(1 1 0) crystallographic planes' ratio (Fig. 7), it was found that it shows a local minimum (BiOBr_Ø), while the exact opposite was found for the hierarchical crystal size. This observation points out two important factors, one of them being that hierarchical entities' size can be increased by decreasing orientated

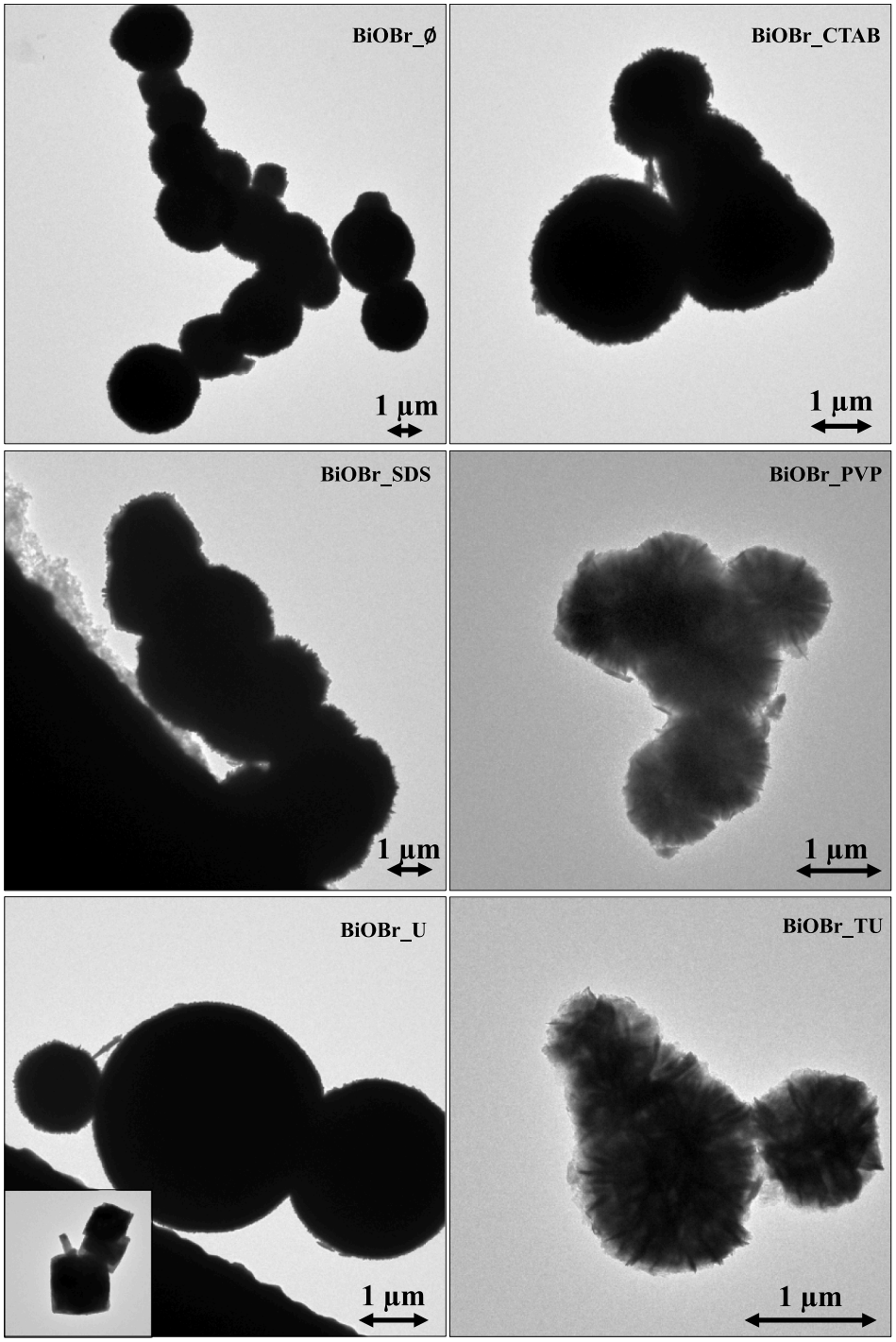

Fig. 3. TEM micrographs of the obtained BiOBr materials, which shows the internal structure of the hierarchical microparticles.

crystal growth, while the other one is the fact that surface tension is a crucial factor to favor hierarchical organization or individual orientated growth of particles. The (1 0 2) and (1 1 0) crystallographic planes ratio may be dependant on the surface tension of the synthesis solution. It could also mean, that the equilibrium could break at a particular surface tension point and if it happens, it could increase the size of hierarchical crystal particles. The crystallization is two-step process: first the nucleation, second the crystal growth. The nucleation of BiOBr is driven by dissociation of the precursors and solvent molecule as the classical nucleation theory describes [37–39]. The individual precursor molecules forms particles overcoming the nucleation barrier. In the surface layer the concentration of the dissociated precursor and solvent molecules are higher, therefore the nucleation barrier and the molecular binding energy could be lower, hence the nucleation rate could be higher, than in the volume. The higher surface tension and lower nucleation barrier at the solution surface could lead easier nucleation of preferred crystal facets [40].

The crystal growth can be treated within the Transition State Theory [41], according to which the reaction rate is higher if the molecule in the initial state (solution) has higher chemical potential. The solvation energy of precursors and solution in the surface layer is increased due to surface tension, so this phenomenon could cause the preferred growth of (1 1 0) crystal facet. Interestingly, no significant correlations were found between the degradation efficiency under visible light/UV light

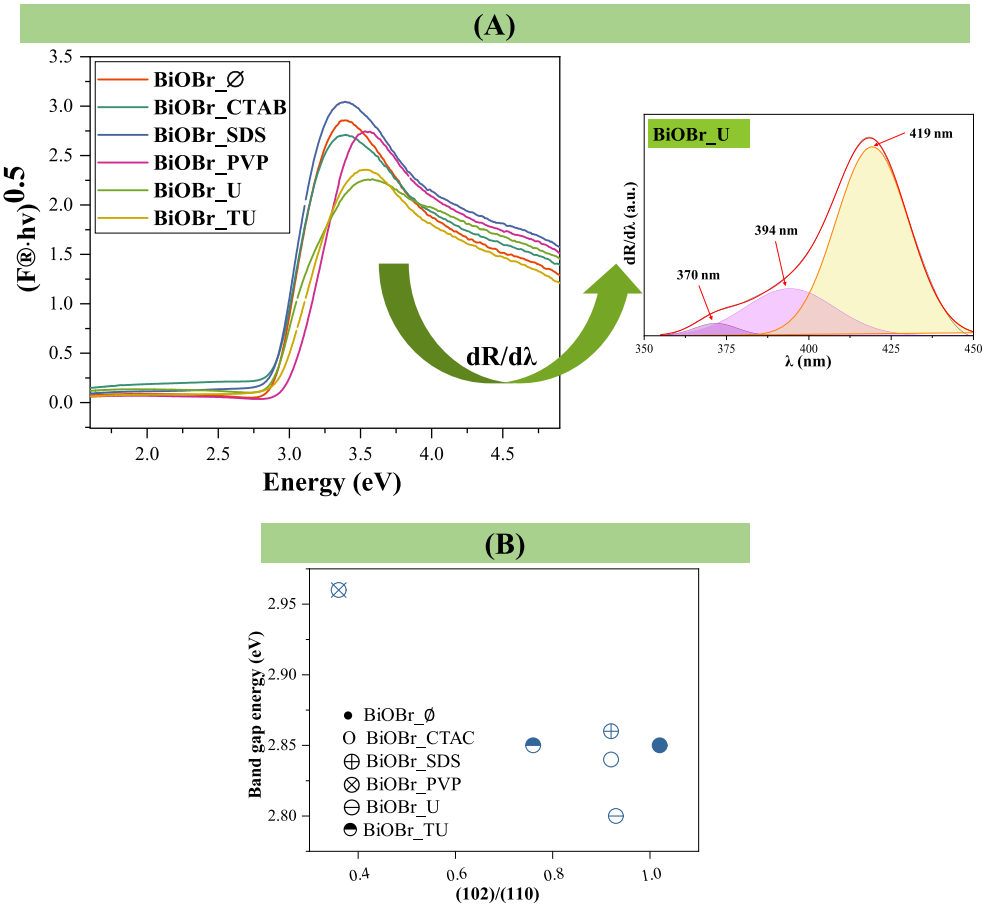

Fig. 4. The diffuse reflectance spectra of the BiOBr materials (A) and the first-order derivative curve of the BiOBr_U sample ((A) *inset*) and the correlation between the band gap energy and the (1 0 2)/(1 1 0) (B) ratios of the crystallographic planes.

irradiation/ band gap energy with the surface tension, pointing out that other parameters were at work here.

The Bi 4f XPS analysis of the samples pointed out fascinating facts (Table 1). Species such as Bi^{3+} (160.1 eV and 165.4 eV), Bi^{4+} (161.4 eV and 166.24 eV) and Bi^{5+} (162.6 eV and 167.6 eV) were identified (Fig. 8). The latter two are rather surprising as they are rare, however not impossible find in the scientific literature. It was already shown, that in $BaBiO_3$ lattice distortions [42] could cause the appearance of Bi^{4+}, while Bi^{5+} was also identified in different mixed BiOX materials and were responsible for the enhanced photocatalytic activity and are considered to participate in electron transfer based photoactivity mechanisms [43]. The band gap was the highest (2.96 eV) where the amount of Bi^{4+} and Bi^{5+} was the highest (16.3% and 7.7%, respectively), in accordance with the UV activity (99%) and specific surface area (41 $m^2 \cdot g^{-1}$) as well – sample BiOBr_PVP. No Bi^{4+} and Bi^{5+}formation were observed when SDS and CTAB were applied and correspondingly their UV activity was low (Table 1). Nevertheless, it seems that alone Bi^{4+} is not sufficient to provide high activity, as in the reference sample, there is a substantial amount of Bi^{4+} but no Bi^{5+}, resulting a lower UV efficiency. Interestingly, the visible light activity did a not show any dependence to the species listed above, which can be explained by the surface sensitization effect, shown by many researchers. Furthermore, it seems that moderate surface tension of the synthesis liquid is required to obtain high concentration of Bi^{4+} and Bi^{5+} (Table 1).

No lower oxidation states were observed in the Bi4f XPS spectra, and the Br3d XPS was unchanged in all the samples, showing the usual signals of Br^- ions in all the BiOBr samples, while the corresponding O1s spectra did not show any signs of oxygen vacancies or any other unusual species.

As it was expected, the ratio of different bismuth species varied with the variation of the synthesis mixtures surface tension. Usually it is expected that, using solvothermal crystallization in the presence of ethylene glycol yields lower oxidation state bismuth, sometimes metallic bismuth as well [44]. However, this is not necessary a rule as in case of other bismuth based photocatalysts, such as Bi_2WO_6, where both higher and lower oxidation states were noticed, due to a partial disproportionation reaction [45]. In the present case it seems that the higher oxidation state will be the dominant, however under special circumstances (Fig. 9).

At lower surface tension values achieved with high efficiency surfactants (samples BiOBr_SDS and BiOBr_CTAB) Bi^{3+} was the only specie detected in the samples. However, as the surface tension values are increasing Bi^{4+} appeared (BiOBr_∅) in 6.8 at.% (FTB[2]). If the surface tension was further increased, the presence of Bi^{4+} was even more pronounced achieving 16.3 at.% (FTB), while 7.7 at.% (FTB) Bi^{5+} was also present (sample BiOBr_PVP). Based on the previous observations it was expected that, further increasing the surface tension value will yield more Bi^{4+} and Bi^{5+}, but it was not case. At even higher surface tension values both Bi^{4+} and Bi^{5+} ratio decreased but did not completely disappeared (samples BiOBr_U and BiOBr_TU).

This suggested clearly that moderate surface tension values are needed to get a higher ratio of the two oxidized bismuth species, while too low or high surface tension values will not lead to success in this regard. This is absolutely important, as the presence of different bismuth entities on the surface of these materials would critically influence their activity and therefore their applicability as well.

[2] FTB-From the total amount of bismuth.

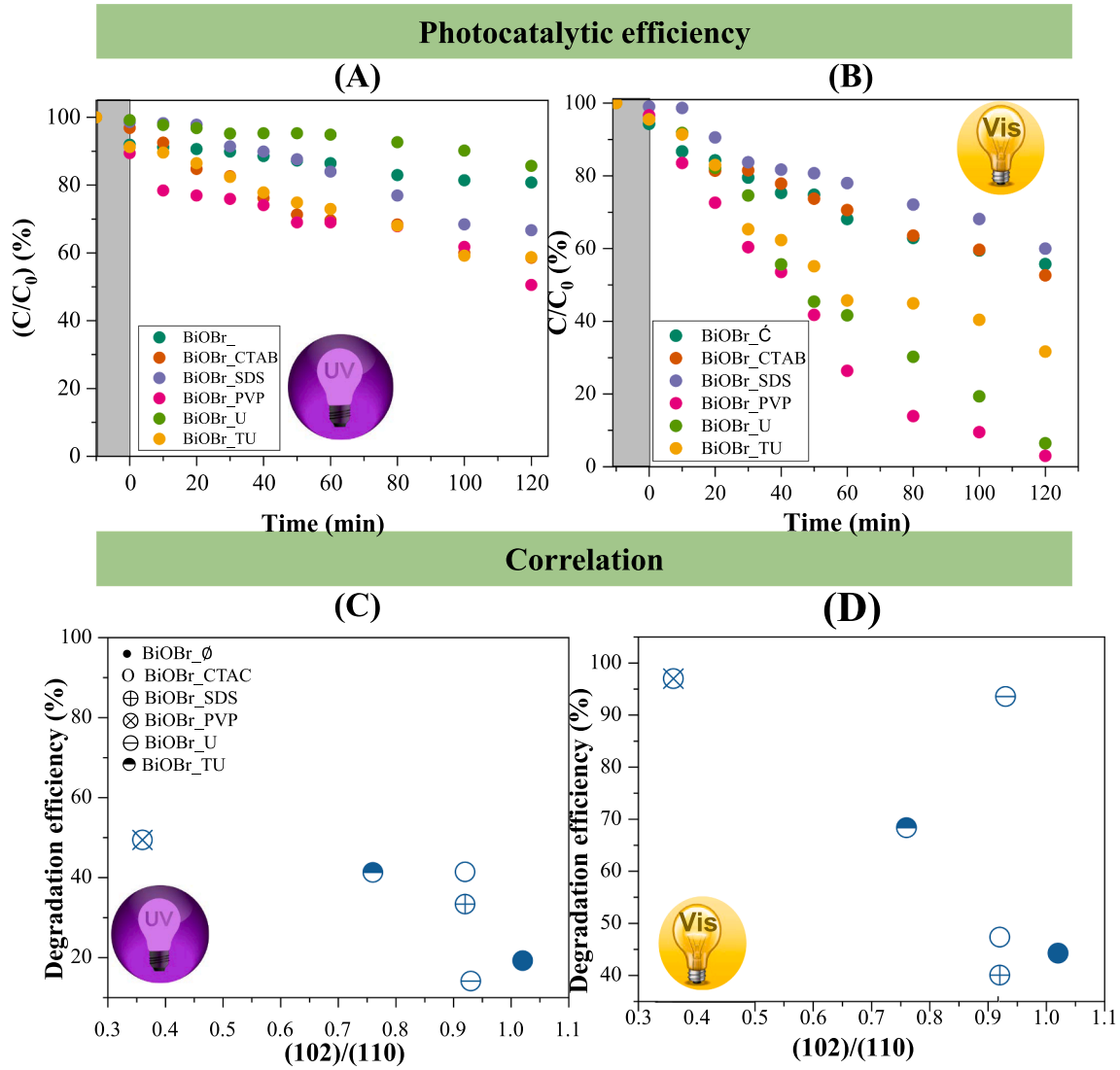

Fig. 5. The photocatalytic activities of BiOBr materials synthesized with different additives under UV (A) and visible light irradiation (B) and the correlation between (1 0 2)/(1 1 0), crystallographic planes ratio under UV (C) and visible light (D).

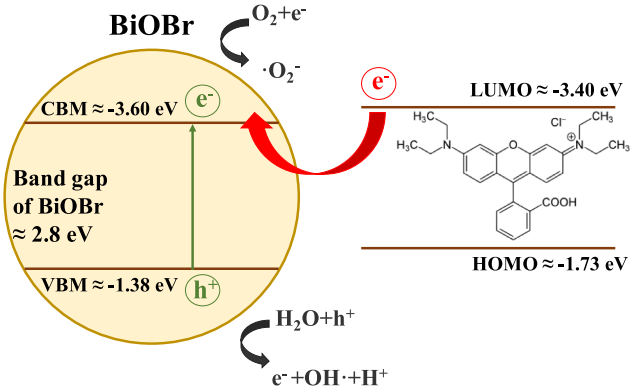

Fig. 6. The illustration of the supposed dye sensitization mechanism.

4. Conclusions

A series of BiOBr samples were successfully synthetized with different additives. From the morphological studies, it was found that all the samples showed hierarchical structures (microspheres, microflowers and microcubes), which were composed of individual crystallites.

It was found that by increasing (1 0 2)/(1 1 0) crystal facets ratio it caused a redshift in the band gap energy of BiOBr materials, which means, that the (1 0 2) crystallographic plane could possess a lower band gap energy. From the DRS measurements, it was found that BiOBr_U contained the formation intermediates $Bi_6O_6(OH)_3(NO_3)_3{\cdot}1.5\ H_2O$ and $Bi_2O_2(OH)(NO)_3$. It was also observed that increasing the (1 0 2)/(1 1 0) ratio decreased the photocatalytic degradation of RhB under UV light irradiation.

The surface tension of the synthesis suspension was responsible for the change in morphological and structural properties, including hierarchical crystal size, mean primary crystallite size, band gap energy and UV light-driven photocatalytic activity. Concomitantly, the surface tension was responsible for the fine-tuning of the Bi^{4+} and Bi^{5+} presence which were also responsible for the photoactivity of the samples. The visible light activity was independent of the factors mentioned above.

CRediT authorship contribution statement

Enikő Bárdos: Investigation, Writing - original draft, Conceptualization. **Viktória Márta:** Investigation. **Lucian Baia:** Formal analysis. **Milica**

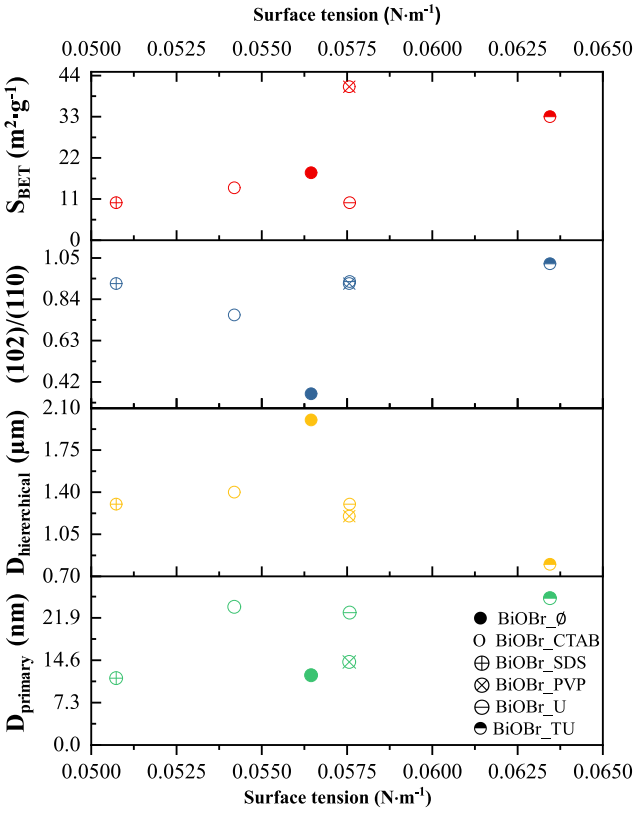

Fig. 7. The influence of surface tension of the synthesis solution on the specific surface area (red), the (1 0 2)/(1 1 0) crystallographic plane ratio (blue), hierarchical crystal size (yellow) and primary crystallite mean size (green). (For interpretation of the references to colour in this figure legend, the reader is referred to the web version of this article.)

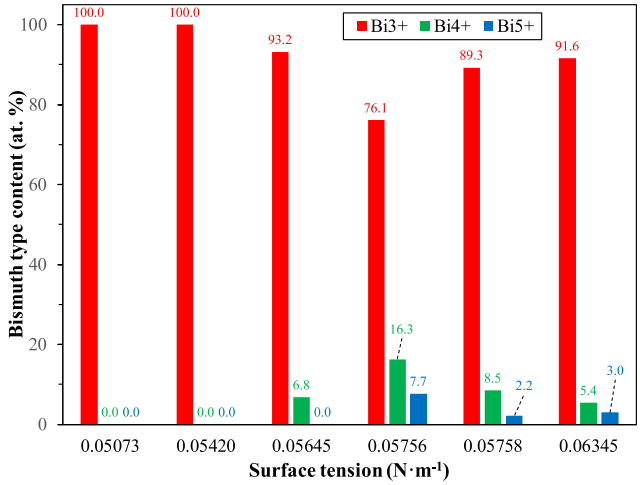

Fig. 9. The surface tension of the synthesis liquid and the resulting bismuth species ratio.

Todea: Investigation. **Gábor Kovács:** Writing - review & editing. **Kornélia Baán:** Investigation. **Seema Garg:** Writing - review & editing. **Zsolt Pap:** Supervision, Writing - original draft. **Klara Hernadi:** Funding acquisition, Writing - review & editing.

Declaration of Competing Interest

The authors declare that they have no known competing financial interests or personal relationships that could have appeared to influence the work reported in this paper.

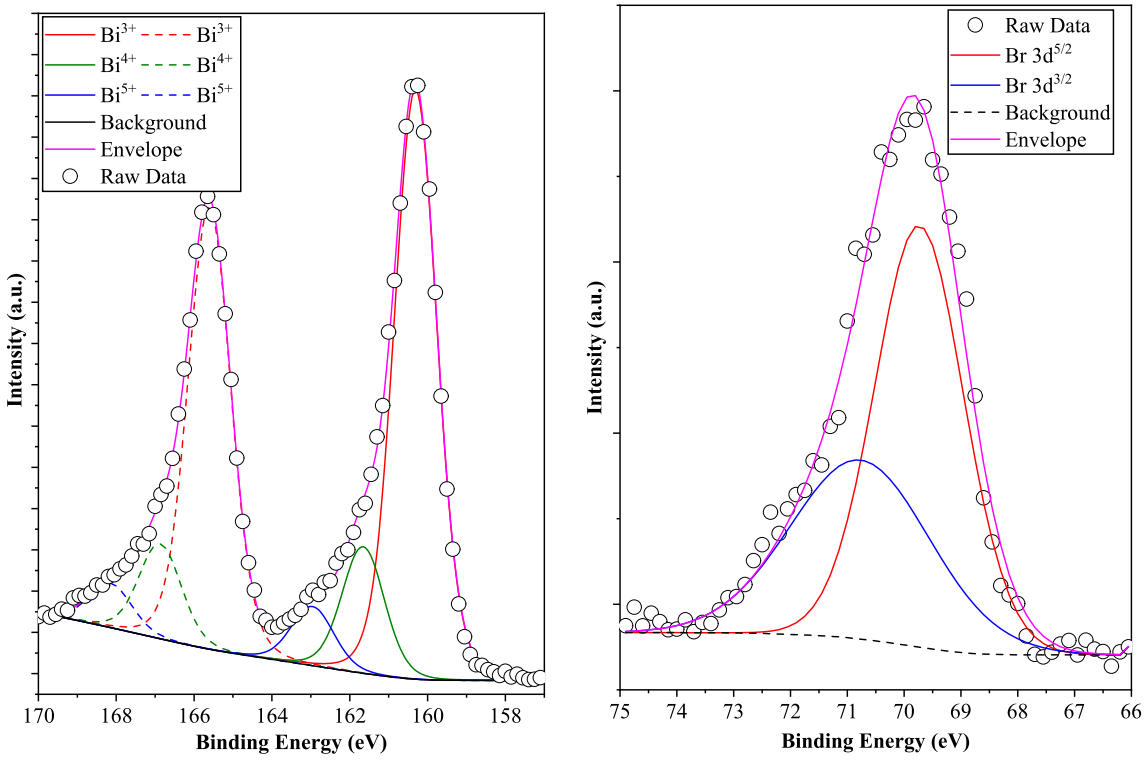

Fig 8. Fitted components in the Bi4f XPS spectrum (left) and Br3d XPS (right) of BiOBr_PVP sample,

Acknowledgment

This work was supported by the Indo-Hungarian TÉT project (TÉT_15_IN-1-2016-0013) and the Department of Science and Technology, Delhi, India (INT/HUN/P-06/2016). Enikő Bárdos would like to express her gratitude to the Campus Mundi Program (EFOP-3.4.2-VEKOP-15-2015-00001), to the New National Excellence Program of the Ministry of Human Capacities (Grant UNKP-19-3) and the Makovecz Program. The authors acknowledge the financial support of NKFI-K-124212 project and Zsolt Pap and Gábor Kovács wishes to thank for the funding provided by the Hungarian Academy of Sciences "Bolyai János Kutatási Ösztöndíj".

Appendix A. Supplementary material

Supplementary data to this article can be found online at https://doi.org/10.1016/j.apsusc.2020.146184.

References

[1] X. Meng, Z. Zhang, Bismuth-based photocatalytic semiconductors: introduction, challenges and possible approaches, J. Mol. Catal. A: Chem. 423 (2016) 533–549, https://doi.org/10.1016/j.molcata.2016.07.030.
[2] Z. Cui, H. Yang, B. Wang, R. Li, X. Wang, Effect of experimental parameters on the hydrothermal synthesis of Bi2WO6 nanostructures, Nanoscale. Res. Lett. 11 (2016) 190, https://doi.org/10.1186/s11671-016-1413-x.
[3] U.M. García-Pérez, A. Martínez-de la Cruz, S. Sepúlveda-Guzmán, J. Peral, Low-temperature synthesis of BiVO4 powders by Pluronic-assisted hydrothermal method: effect of the surfactant and temperature on the morphology and structural control, Ceram. Int. 40 (2014) 4631–4638, https://doi.org/10.1016/j.ceramint.2013.09.002.
[4] A. Martínez-de la Cruz, S. Obregón Alfaro, E. López Cuéllar, U. Ortiz Méndez, Photocatalytic properties of Bi2MoO6 nanoparticles prepared by an amorphous complex precursor, Catal. Today 129 (2007) 194–199, https://doi.org/10.1016/j.cattod.2007.08.004.
[5] Y. Yang, C. Zhang, C. Lai, G. Zeng, D. Huang, M. Cheng, J. Wang, F. Chen, C. Zhou, W. Xiong, BiOX (X = Cl, Br, I) photocatalytic nanomaterials: applications for fuels and environmental management, Adv. Colloid Interface Sci. 254 (2018) 76–93, https://doi.org/10.1016/j.cis.2018.03.004.
[6] S. Garg, M. Yadav, A. Chandra, S. Sapra, S. Gahlawat, P.P. Ingole, M. Todea, E. Bardos, Z. Pap, K. Hernadi, Facile green synthesis of BiOBr nanostructures with superior visible-light-driven photocatalytic activity, Materials 11 (2018), https://doi.org/10.3390/ma11081273.
[7] W.L. Huang, Electronic structures and optical properties of BiOX (X = F, Cl, Br, I) via DFT calculations, J. Comput. Chem. 30 (2009) 1882–1891, https://doi.org/10.1002/jcc.21191.
[8] L. Zhao, X. Zhang, C. Fan, Z. Liang, P. Han, First-principles study on the structural, electronic and optical properties of BiOX (X = Cl, Br, I) crystals, Physica B: Condensed Matter 407 (2012) 3364–3370, https://doi.org/10.1016/j.physb.2012.04.039.
[9] S. Garg, M. Yadav, A. Chandra, K. Hernadi, A review on BiOX (X = Cl, Br and I) nano-/microstructures for their photocatalytic applications, J. Nanosci. Nanotechnol. 19 (2019) 280–294, https://doi.org/10.1166/jnn.2019.15771.
[10] H. Zhang, Y. Yang, Z. Zhou, Y. Zhao, L. Liu, Enhanced photocatalytic properties in BiOBr nanosheets with dominantly exposed (102) facets, J. Phys. Chem. C 118 (2014) 14662–14669, https://doi.org/10.1021/jp5035079.
[11] X. Wu, Y.H. Ng, L. Wang, Y. Du, S.X. Dou, R. Amal, J. Scott, Improving the photooxidative capability of BiOBr via crystal facet engineering, J. Mater. Chem. A Chem. 5 (2017) 8117–8124, https://doi.org/10.1039/c6ta10964k.
[12] P. Panudda, N. Ekthammathat, A. Phuruangrat, S. Thongtem, T. Thongtem, BiOX (X = Cl, Br, and I) nanoplates prepared by surfactant-free microwave synthesis and their photocatalytic performance, Russ. J. Phys. Chem. A 92 (2018) 2289–2295, https://doi.org/10.1134/s0036024418110328.
[13] D. Zhang, J. Li, Q. Wang, Q. Wu, High 001 facets dominated BiOBr lamellas: facile hydrolysis preparation and selective visible-light photocatalytic activity, J. Mater. Chem. AChem 1 (2013) 8622, https://doi.org/10.1039/c3ta11390f.
[14] Y. Liu, Y. Yin, X. Jia, X. Cui, C. Tian, Y. Sang, H. Liu, Synthesis process and photocatalytic properties of BiOBr nanosheets for gaseous benzene, Environ. Sci. Pollut. Res. Int. 23 (2016) 17525–17531, https://doi.org/10.1007/s11356-016-6951-3.
[15] S. Duo, Y. Li, H. Zhang, T. Liu, K. Wu, Z. Li, A facile salicylic acid assisted hydrothermal synthesis of different flower-like ZnO hierarchical architectures with optical and concentration-dependent photocatalytic properties, Mater. Charact. 114 (2016) 185–196, https://doi.org/10.1016/j.matchar.2016.02.021.
[16] R. Miao, W. Zeng, Q. Gao, Hydrothermal synthesis of novel NiO nanoflowers assisted with CTAB and SDS respectively and their gas-sensing properties, Mater. Lett. 186 (2017) 175–177, https://doi.org/10.1016/j.matlet.2016.09.127.
[17] Z. Zhu, J. Du, J. Li, Y. Zhang, D. Liu, An EDTA-assisted hydrothermal synthesis of BiVO4 hollow microspheres and their evolution into nanocages, Ceram. Int. 38 (2012) 4827–4834, https://doi.org/10.1016/j.ceramint.2012.02.071.
[18] M.M. Rashad, A.E. Shalan, Surfactant-assisted hydrothermal synthesis of titania nanoparticles for solar cell applications, J. Mater. Sci. - Mater. Electron. 24 (2013) 3189–3194, https://doi.org/10.1007/s10854-013-1226-y.
[19] S. Fodor, L. Baia, M. Focșan, K. Hernádi, Z. Pap, Designed and controlled synthesis of visible light active copper(I)oxide photocatalyst: from cubes towards the polyhedrons - with Cu nanoparticles, App. Sur. Sci. 484 (2019) 175–183, https://doi.org/10.1016/j.apsusc.2019.03.288.
[20] W. Yin, W. Wang, L. Zhou, S. Sun, L. Zhang, CTAB-assisted synthesis of monoclinic BiVO4 photocatalyst and its highly efficient degradation of organic dye under visible-light irradiation, J. Hazard. Mater. 173 (2010) 194–199, https://doi.org/10.1016/j.jhazmat.2009.08.068.
[21] X. Shi, X. Chen, S. Zhou, S. Lou, Y. Wang, L. Yuan, PVP assisted hydrothermal synthesis of BiOBr hierarchical nanostructures and high photocatalytic capacity, Chem. Eng. J. 222 (2013) 120–127, https://doi.org/10.1016/j.cej.2013.02.034.
[22] Y. Yang, L. Geng, Y. Guo, Y. Guo, Morphology evolution and excellent visible-light photocatalytic activity of BiOBr hollow microspheres, J. Chem. Technol. Biotechnol. 92 (2017) 1236–1247, https://doi.org/10.1002/jctb.5117.
[23] Y. Zhao, X. Tan, T. Yu, S. Wang, SDS-assisted solvothermal synthesis of BiOBr microspheres with highly visible-light photocatalytic activity, Mater. Lett. 164 (2016) 243–247, https://doi.org/10.1016/j.matlet.2015.10.155.
[24] H.-T. Wang, M.-S. Shi, H.-F. Yang, N. Chang, H. Zhang, Y.-P. Liu, M.-C. Lu, D. Ao, D.-Q. Chu, Template-free synthesis of nanosliced BiOBr hollow microspheres with high surface area and efficient photocatalytic activity, Mater. Lett. 222 (2018) 164–167, https://doi.org/10.1016/j.matlet.2018.03.179.
[25] M. Shang, W. Wang, L. Zhang, Preparation of BiOBr lamellar structure with high photocatalytic activity by CTAB as Br source and template, J. Hazard. Mater. 167 (2009) 803–809, https://doi.org/10.1016/j.jhazmat.2009.01.053.
[26] Q. Han, K. Zhang, J. Zhang, S. Gong, X. Wang, J. Zhu, Effect of the counter ions on composition and morphology of bismuth oxyhalides and their photocatalytic performance, Chem. Eng. J. 299 (2016) 217–226, https://doi.org/10.1016/j.cej.2016.04.048.
[27] M. Song, M. Du, Q. Liu, F. Xing, C. Huang, X. Qiu, Enhancement of photocatalytic activities in hierarchical BiOBr microflowers induced by oxygen vacancies, Catal. Today 335 (2019) 193–199, https://doi.org/10.1016/j.cattod.2018.11.006.
[28] G.-H. Jiang, X. Li, Z. Wei, T.-T. Jiang, X.-X. Du, W.-X. Chen, Effects of N and/or S doping on structure and photocatalytic properties of BiOBr crystals, Acta Metallurgica Sinica (Engl. Lett.) 28 (2015) 460–466, https://doi.org/10.1007/s40195-015-0220-1.
[29] Z. Kása, L. Baia, K. Magyari, K. Hernádi, Z. Pap, Innovative visualization of the effects of crystal morphology on semiconductor photocatalysts. Tuning the Hückel polarity of the shape-tailoring agents: the case of Bi2WO6, Cryst. Eng. Comm. 21 (2019) 1267–1278, https://doi.org/10.1039/c8ce01744a.
[30] P. Kubelka, F. Munk, Ein Beitrag Zur Optik Der Farbanstriche, Zeitschrift für Technische Physik 12 (1931) 593–601.
[31] R. Jenkins, R.L. Snyder, Introduction to X-Ray Powder Diffractometry, John Wiley & Sons, New York, 1996.
[32] M. Meire, S.W. Verbruggen, S. Lenaerts, P. Lommens, P. Van Der Voort, I. Van Driessche, Microwave-assisted synthesis of mesoporous titania with increased crystallinity, specific surface area, and photocatalytic activity, J. Mater. Sci 51 (2016) 9822–9829, https://doi.org/10.1007/s10853-016-0215-y.
[33] L.-M. Yang, G.-Y. Zhang, Y. Liu, Y.-Y. Xu, C.-M. Liu, J.-W. Liu, A 110 facet predominated Bi6O6(OH)3(NO3)3·1.5H2O photocatalyst: selective hydrothermal synthesis and its superior photocatalytic activity for degradation of phenol, RSC Adv. 5 (2015) 79715–79723, https://doi.org/10.1039/c5ra15629g.
[34] Y. Yang, H. Liang, N. Zhu, Y. Zhao, C. Guo, L. Liu, New type of [Bi6O6(OH)3](NO3) 3.1.5H2O sheets photocatalyst with high photocatalytic activity on degradation of phenol, Chemosphere 93 (2013) 701–707, https://doi.org/10.1016/j.chemosphere.2013.06.062.
[35] Q. Han, J. Pang, X. Wang, X. Wu, J. Zhu, Synthesis of unique flowerlike Bi2 O2 (OH) (NO3) hierarchical microstructures with high surface area and superior photocatalytic performance, Chemistry 23 (2017) 3891–3897, https://doi.org/10.1002/chem.201604085.
[36] N. Sharma, Z. Pap, S. Garg, K. Hernádi, Hydrothermal synthesis of BiOBr and BiOBr/CNT composites, their photocatalytic activity and the importance of early Bi6O6(OH)3(NO3)3·1.5H2O formation, App. Sur. Sci. 495 (2019) 143536, , https://doi.org/10.1016/j.apsusc.2019.143536.
[37] R. Becker, W. Doring, Annalen der Physik 416 (1935) 719–752, https://doi.org/10.1002/andp.19354160806.
[38] M. Volmer, A. Weber, Zeitschrift für Physikalische Chemie 119 (1926) 277–301, https://doi.org/10.1515/zpch-1926-11927.
[39] D.R. Cassar, Solving the classical nucleation theory with respect to the surface energy, J. Non-Cryst. Solids 511 (2019) 183–185, https://doi.org/10.1016/j.jnoncrysol.2019.02.006.
[40] A.A. Zhumekenov, V.M. Burlakov, M.I. Saidaminov, A. Alofi, M.A. Haque, B. Turedi, B. Davaasuren, I. Dursun, N. Cho, A.M. El-Zohry, M.D. Bastiani, A. Giugni, B. Torre, E.D. Fabrizio, O.F. Mohammed, A. Rothenberger, T. Wu, A. Goriely, O.M. Bakr, The role of surface tension in the crystallization of metal halide perovskites, ACS Energy Lett. 2 (2017) 1782–1788, https://doi.org/10.1021/acsenergylett.7b00468.
[41] J.F. Oliver, C. Huh, S.G. Mason, Resistance to spreading of liquids by sharp edges, J. Colloid Interface Sci. 59 (1977).
[42] D. Korotin, V. Kukolev, A.V. Kozhevnikov, D. Novoselov, V.I. Anisimov, Electronic correlations and crystal structure distortions in BaBiO3, J. Phys.: Condens. Matter 24 (2012) 415603, , https://doi.org/10.1088/0953-8984/24/41/415603.
[43] G. Zhang, L. Cai, Y. Zhang, Y. Wei, Bi(5+), Bi((3–x)+), and oxygen vacancy induced BiOClx I1–x solid solution toward promoting visible-light driven photocatalytic activity, Chemistry 24 (2018) 7434–7444, https://doi.org/10.1002/chem.201706164.
[44] E. Bárdos, A.K. Király, Z. Pap, L. Baia, S. Garg, K. Hernádi, The effect of the synthesis temperature and duration on the morphology and photocatalytic activity of BiOX (X = Cl, Br, I) materials, Appl. Surf. Sci. 479 (2019) 745–756, https://doi.org/10.1016/j.apsusc.2019.02.136.
[45] Z. Kása, K. Saszet, A. Dombi, K. Hernádi, L. Baia, K. Magyari, Z. Pap, Thiourea and Triton X-100 as shape manipulating tools or more for Bi 2 WO 6 photocatalysts? Mater. Sci. Semicond. Process. 74 (2018) 21–30, https://doi.org/10.1016/j.mssp.2017.10.001.